Polarization Modulation Fourier Transform Infrared Reflectance Measurements of Thin Films and Monolayers at Metal Surfaces Utilizing Real-Time Sampling Electronics

Barbara J. Barner, Michael J. Green, Edna I. Sáez, and Robert M. Corn*

Department of Chemistry, University of Wisconsin, 1101 University Avenue, Madison, Wisconsin 53706

The technique of polarization modulation Fourier transform infrared (PM-FTIR) spectroscopy is applied to the reflectance spectra of thin polymer films and spontaneously organized monolayers adsorbed onto gold, silver, and chromium surfaces. The differential PM-FTIR reflectance spectra are obtained by the photoelastic modulation of the FTIR beam polarization and a novel real-time sampling methodology that generates the average and differential FTIR interferograms from measurements of the infrared signal during each modulation cycle. In comparison with conventional electronics that utilize a lock-in amplifier, the real-time electronics permit the operation of the FTIR spectrometer at normal mirror velocities. The use of polarization-independent optics after the metal surface ensures that the true surface infrared differential reflectance spectrum is obtained. The theoretical wavelength dependence of the PM-FTIR spectrum is rederived for the case of the real-time sampling measurement and compared to the experimental data. Spectra of a 15-nm film of polyimide on chromium, a spontaneously organized monolayer of octadecanethiol on gold, and a spontaneously organized monolayer of arachidic acid on silver are shown to demonstrate the applicability of the method to different metals, samples, and spectral regions.

I. INTRODUCTION

Infrared reflectance spectroscopy has developed into one of the primary methods of monitoring the chemical structure and molecular orientation of thin films and monolayers adsorbed onto metal surfaces (*1, 2*). At a high (grazing) angle of incidence, the intensity of a reflected p-polarized infrared light beam is enhanced at a metal surface so that even submonolayer quantities of chemisorbed species can be observed in the p-polarized FTIR reflectance spectrum (*3*). In contrast, at a high angle of incidence, an s-polarized reflected infrared beam has virtually no intensity at the metal surface. This polarization disparity leads to strong selection rules at the surface and has been used to deduce the average molecular orientation and conformation for monolayers of long-chain alkyl molecules adsorbed onto metals (*4–7*).

In addition to orientation measurements, the predominance of p-polarized light over s-polarized light at the metal surface has been utilized to obtain the differential reflectance spectrum of the adsorbed surface species, $\Delta R/R$, by polarization modulation of the infrared light (*8–14*). Differential reflectance measurements have been obtained with both scanning spectrometers (*9, 10*) and FTIR instruments (*11–13*); the FTIR instruments have the advantage of very good resolution, rapid acquisition time, and a wide spectral range (*8*). The differential reflectance measurement possesses an inherent surface sensitivity that makes it an ideal technique for in situ studies at condensed-phase interfaces such as electrochemical surfaces (*14*).

Although PM-FTIR spectroscopy has been successfully employed in a number of environments, the measurements from metal surfaces to date have been restricted by some experimental limitations to this modulation technique. Current implementations of the PM-FTIR scheme utilize a lock-in amplifier to extract the differential interferogram from the detector signal (*8*). In order to ensure that the variations in the differential signal do not exceed the time constant of the lock-in amplifier output electronics, the mirror velocity is typically slowed down, reducing the stability of the interferometer and diminishing the signal averaging capabilities of the instrument. In addition, the spectral window of the PM-FTIR reflectance spectrum is modulated by the wavelength dependence of the photoelastic polarization modulator. A background spectrum is typically taken to subtract off this variation as well as any other instrumental artifacts (*11–13*). This paper describes how to obtain the PM-FTIR differential reflectance spectrum at normal mirror velocities and demonstrates how in some cases the need for a background spectrum can be avoided through appropriate collection optics and knowledge of the theoretical PM-FTIR wavelength dependence. The utility of the method is demonstrated for various thin film and monolayer samples at a variety of metal surfaces.

II. EXPERIMENTAL CONSIDERATIONS

The FTIR instrument employed in these experiments is a Mattson Cygnus 100 FTIR spectrometer. The optical layout for the reflectance measurement is depicted in Figure 1. The entire experimental layout was enclosed in a nitrogen purge box to avoid sample contamination. The FTIR beam was focused onto the sample at an incident angle of 75°, creating an elliptical spot size of approximately 7 mm × 10 mm. Prior to the sample, the FTIR beam passed through a wire grid polarizer (Molectron), creating a p-polarized beam that was then sent through a ZnSe photoelastic modulator (PEM, Hinds). After the sample, the infrared beam was collected with a single ZnSe lens and focused onto a HgCdTe detector. It was important to have only polarization-insensitive elements after the sample, since any instrumental polarization differences will appear in the PM-FTIR spectrum. For characterization purposes, the detector output was recorded and analyzed with a digital oscilloscope (Le Croy 9400). To obtain a differential reflectance measurement, the detector signal was sent to specialized electronics (described briefly below and in detail elsewhere (*15*)) that generated the average and difference interferograms required for the PM-FTIR spectrum. The interferograms were then digitized with the A/D converters of the instrument and processed. All spectra were obtained at a nominal resolution of 2 cm^{-1}.

Three samples were prepared to test the sensitivity and viability of the PM-FTIR experiments. A thin polyimide film sample was created by spin-coating and thermally annealing a 15-nm film of polyamic acid on a Cr-coated Si substrate. The polyamic acid film (Du Pont, PI 2545) was deposited onto the substrate by spin-coating at 4000 rpm from a 2% solution in *N*-methylpyrrolidinone. The sample was dried at 120 °C to remove the solvent and then cyclized thermally at 300 °C. The thickness of the resultant polyimide thin film was measured with profilometry. An organized monolayer sample was created by the adsorption

0003-2700/91/0363-0055$02.50/0 © 1990 American Chemical Society

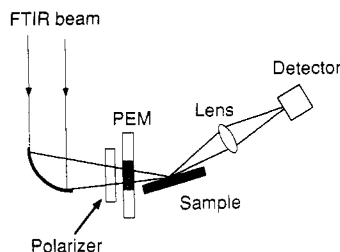

Figure 1. Optical layout of the PM-FTIR experiment. The polarizer creates a p-polarized incident beam on the sample that is polarization-modulated by the PEM. The use of a single lens prior to the detector ensures that the PM-FTIR differential reflectance spectrum obtained is solely from the sample.

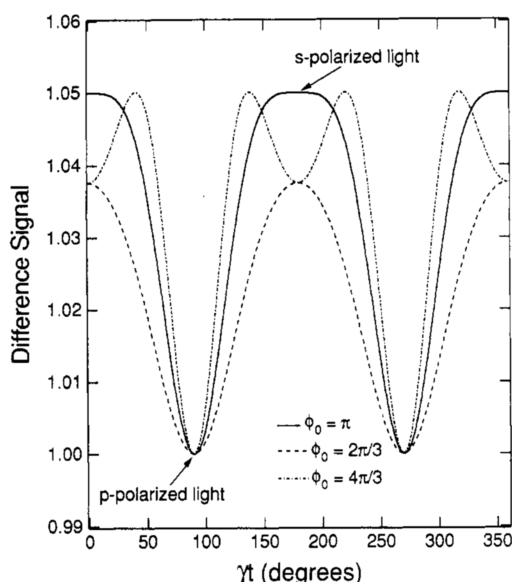

Figure 2. Theoretical curves for a monochromatic real-time reflectance signal from a sample that is 5% more reflective for s-polarized light than for p-polarized light. The modulated signal depends upon the constant ϕ_0, which varies linearly with wavenumber (see text).

of a 1-octadecanethiol ($C_{18}H_{37}SH$, Fluka) monolayer onto a polycrystalline gold plug from a 1 mM methylene chloride solution. Prior to adsorption, the gold plug was cleaned first with a peroxide rinse and then electrochemically. A second organized monolayer sample was created by the adsorption of a spontaneously organized arachidic acid ($C_{19}H_{39}COOH$, Sigma) monolayer from a 1 mM carbon tetrachloride solution onto a vapor-deposited 300-nm silver film. Deposition occurred immediately after formation of the silver films on a Si substrate by a turbomolecular-pumped vacuum deposition apparatus (Balzers).

III. PM-FTIR THEORY AND INSTRUMENTATION

Polarization Modulation Equations. The PEM modulates the infrared beam by rotating the polarization of the light sinusoidally at the frequency of the birefringence introduced mechanically in the ZnSe crystal. If a monochromatic incident infrared beam that is linearly polarized 45° to the strain axis is passed through the modulator, the intensity of output light is given by *(16)*

$$I(t) = [I_p + I_s + (I_p - I_s) \cos (\phi_0 \cos (\gamma t))]/2 \quad (1)$$

where I_p is the polarization of the beam prior to passage through the modulator and is experimentally set to p-polarized light relative to the sample surface (i.e., polarized so that the electric field is parallel to the plane of incidence of the incident and reflected infrared beams off the metal surface), I_s is s-polarized light relative to the sample surface (i.e., polarized so that the electric field is perpendicular to the plane of incidence), $\cos (\gamma t)$ is set to a modulation frequency of 37 kHz,

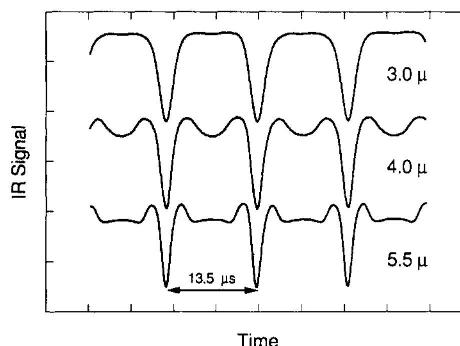

Figure 3. Experimental real-time reflectance signals of the polarization-modulated interferometer beam on a vapor-deposited polycrystalline gold sample (the moving mirror of the interferometer is fixed at a point away from the zero path difference for these measurements). Three curves are shown corresponding to PEM voltages set such that $\phi_0 = \pi$ for wavelengths of 3.0, 4.0, and 5.5 μm.

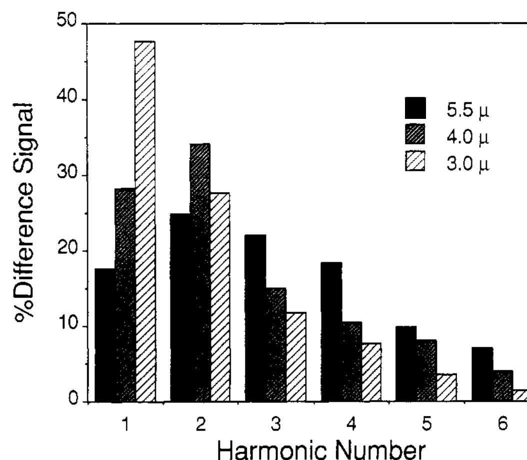

Figure 4. Fourier analysis of the real-time reflectance signals shown in Figure 3. The harmonic number corresponds to multiples of 74 kHz, the second harmonic of the modulation frequency of the ZnSe crystal.

and the constant ϕ_0 depends linearly on the voltage of the applied modulation and is inversely related to the wavelength of the light ($\phi_0 = GV_m/\lambda$). If the voltage is set such that $\phi_0 = \pi$ for a particular wavelength, then when γt is equal to 90° or 270°, $I(t) = I_p$, and when γt is equal to 0° or 180°, $I(t) = I_s$. The theoretical $I(t)$ curve for $\phi_0 = \pi$ is plotted in Figure 2. The effective modulation frequency is twice the oscillation frequency, or 74 kHz. For scanning spectrometers, the voltage applied to the crystal can be varied continuously during a wavelength scan so that ϕ_0 is always set to π. However, in the FTIR measurement, all of the wavelengths of the spectrometer are present simultaneously during the interferogram. In this case, $\phi_0 \neq \pi$ in general and $I(t)$ at 0°, 90°, 180°, and 270° is given by

$$I(t) = I_p \qquad \gamma t = 90°, 270° \quad (2)$$

$$I(t) = \text{“}I_s\text{”} = I_s + (I_p - I_s)(1 + \cos \phi_0)/2 \qquad \gamma t = 0°, 180° \quad (3)$$

The theoretical curves for the PM waveform when $\phi_0 = 2\pi/3$ and $4\pi/3$ are also shown in Figure 2. Note that if the PEM rotates the polarization too much or too little, the result is the same: the modulation at 74 kHz is decreased by an amount proportional to $I_p - I_s$. The experimentally observed waveform for the FTIR beam reflected off of a gold surface is shown in Figure 3 for voltage settings where $\phi_0 = \pi$ at wavelengths of 3.0, 4.0, and 5.5 μm. These waveforms are a sum of $I(t)$ waveforms for all of the different wavelengths present in the interferogram, weighted by the throughput and response of the spectrometer and detector.

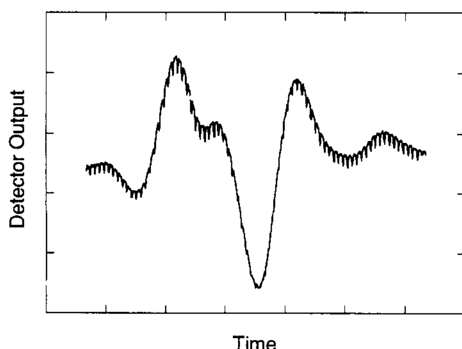

Figure 5. Portion of the experimental PM-FTIR interferogram signal obtained prior to the real-time sampling electronics. The small negative spikes on the interferogram are from the polarization modulation. The height of these spikes is the differential PM-FTIR measurement and must be obtained in the presence of the relatively large variations in the average interferogram signal.

A Fourier analysis of the infrared waveforms at the three voltage settings is shown in Figure 4. Virtually all of the power in the waveform can be accounted for with the first six harmonics of 74 kHz. As depicted in Figure 4, the experimental waveforms all contain a substantial percentage of modulation at harmonics above 74 kHz. Previous implementations of PM-FTIR spectroscopy have employed a lock-in amplifier to obtain the modulation response at 74 kHz. Unfortunately, these spectra are limited by the time constant of the lock-in amplifier output electronics, which are normally on the order of 0.5 ms. This time constant requires that the mirror velocity of the interferometer must be slowed down so that the modulation frequencies in the interferogram fall below 2 kHz. Most FTIR spectrometers are designed to operate at mirror velocities on the order of 10–15 times higher than this cutoff value. Spectrometers with variable mirror velocities are capable of running at velocities sufficiently low for this experiment; however, they are in general much less stable when running at these speeds. Of course, the signal averaging capabilities of the FTIR are directly affected by the reduced mirror scan rate as well.

To avoid these problems, real-time sampling electronics were designed to measure $I(t)$ at 0° and 90° during each modulation cycle. This direct measurement of I_p and "I_s" enabled the analysis of interferograms up to frequencies of 10–20 kHz and thus permitted the interferometer mirror to be scanned at normal velocities. One complication that arises is that because $I(t)$ is being sampled during an interferogram, I_p and "I_s" are now functions of mirror displacement, so that the functions $I_p(\delta)$ and "I_s"(δ) are continually changing as a function of time (see Figure 5). In principle, one would like to measure $I_p(\delta)$ and "I_s"(δ) simultaneously. The simultaneous measurement of I_p and "I_s" can be estimated by a quadratic approximation method depicted in Figure 6. At γt = 90°, the interferogram is sampled to obtain an I_p measurement. The "I_s" measurement at 90° is approximated by a Taylor series expansion about "I_s" at 0°

$$\text{“}I_s\text{”}(\gamma t = 90°) \approx \text{“}I_s\text{”}(0°) + f'\Delta[\gamma t] + f''\Delta[\gamma t]^2/2 \quad (4)$$

where the first and second derivative terms $f'\Delta[\gamma t]$ and $f''\Delta[\gamma t]^2/2$ are obtained from measurements of "I_s" at −180° and 180°:

$$f'\Delta[\gamma t] = [\text{“}I_s\text{”}(180°) - \text{“}I_s\text{”}(0°)]/2 \quad (5)$$

$$f''\Delta[\gamma t]^2/2 = [\text{“}I_s\text{”}(180°) - 2\text{“}I_s\text{”}(0°) + \text{“}I_s\text{”}(-180°)]/8 \quad (6)$$

The real-time sampling electronics generate an average and a difference interferogram $I_A(\delta) = (I_p(\delta) + \text{“}I_s\text{”}(\delta))/2$ and $I_D(\delta) = I_p(\delta) - \text{“}I_s\text{”}(\delta)$, respectively. The difference interferogram

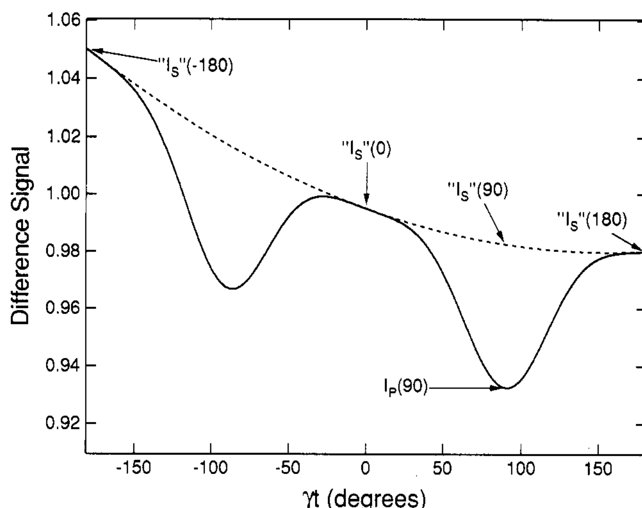

Figure 6. Methodology for sampling the real-time modulation signals I_p and "I_s" during an interferogram. The value of I_p is measured directly at 90°, and the value of "I_s"(90) is estimated from the three points "I_s"(−180), "I_s"(90), and "I_s"(180). See text for details.

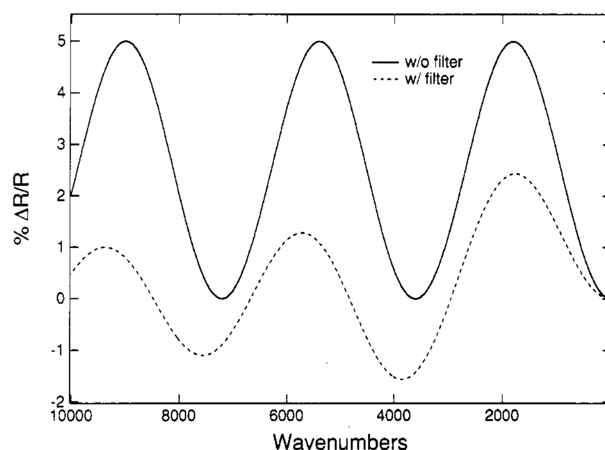

Figure 7. Theoretical PM-FTIR differential reflectance spectrum of a sample with a wavelength-independent reflectivity difference of 5%. The solid curve is the wavelength dependence expected from the real-time sampling electronics, and the dotted curve is the wavelength dependence expected if only the second harmonic is employed.

is typically 10–40 times smaller than the average interferogram and is amplified to a comparable signal level. These two interferograms are then digitized in alternating blocks of mirror scans with the A/D converter of the spectrometer and Fourier transformed to yield the two spectra $I_A(\omega)$ and $I_D(\omega)$, respectively,

$$I_A(\omega) = (I_p(\omega) + \text{“}I_s\text{”}(\omega))/2 = \langle I(\omega)\rangle + \Delta I(\omega)(1 + \cos\phi_0)/4 \quad (7)$$

$$I_D(\omega) = I_p(\omega) - \text{“}I_s\text{”}(\omega) = \Delta I(\omega)(1 - \cos\phi_0)/2 \quad (8)$$

where $\Delta I(\omega) \equiv I_p(\omega) - I_s(\omega)$ and $\langle I(\omega)\rangle \equiv (I_p(\omega) + I_s(\omega))/2$. From these two spectra, the differential reflectance spectrum $\Delta R/R \equiv I_D(\omega)/I_A(\omega)$ is formed:

$$\Delta R/R \approx [(1 - \cos\phi_0)/2 - (\Delta I(\omega)/\langle I(\omega)\rangle) \times (\sin^2\phi_0)/8]\Delta I(\omega)/\langle I(\omega)\rangle \quad (9)$$

Equation 9 demonstrates that with the PM-FTIR measurement the true reflectance spectrum $\Delta I/\langle I\rangle$ is obtained times a term that, if $\Delta I/\langle I\rangle$ is small, looks like $(1 - \cos\phi_0)/2$. The phase shift ϕ_0 varies linearly with frequency, yielding a theoretical background variation in $\Delta R/R$ that should be discernible experimentally. A theoretical differential reflectance spectrum is plotted in Figure 7 for the case where $\Delta I/\langle I\rangle$ is independent of wavelength and equal to 5%.

The functional form of the differential reflectance spectrum obtained with the real-time sampling electronics varies slightly from that obtained in previous implementations of the PM-FTIR experiments. In those studies, only the modulation at the second harmonic frequency (74 kHz) was measured. Hipps and Crosby (*16*) have shown that the differential reflectance spectrum obtained in this manner will have the form

$$\Delta R/R \approx J_2(\phi_0)\Delta I(\omega)/\langle I(\omega)\rangle \quad (10)$$

where $J_2(\phi_0)$ is the second-order Bessel function. A theoretical differential reflectance spectrum for this measurement is plotted along with the real-time sampling case in Figure 7. The use of only the second harmonic response decreases the magnitude of the differential reflectance spectrum by an amount depicted graphically in Figure 4. However, the signal measurement at 2ω is normally filtered to yield a reduced bandwidth that results in the substantial rejection of any extraneous noise signals. The second harmonic measurement was also obtained with the real-time sampling electronics (at normal mirror velocities) by the insertion of two 5-pole filters at 50 and 100 kHz into the difference signal channel. In this case, the resulting differential reflectance spectrum is expected to display the functional form of eq 10 in lieu of eq 9.

IV. RESULTS AND DISCUSSION

To demonstrate the viability of the real-time PM-FTIR measurement, the differential reflectance spectrum obtained from a 15-nm polyimide film deposited onto a Cr substrate is shown in Figure 8. Figure 8A plots $-(\%\ \Delta R/R)$ from 750 to 7899 cm^{-1} to display the functional form of the spectrum introduced by the PEM, which was set such that $\phi_0 = \pi$ at 5.50 μm. This functional waveform roughly matches the sinusoidal dependence predicted by eq 9 and plotted in Figure 7. The reflectance spectrum in Figure 8A was obtained after application of a phase correction to $I_D(\omega)$ that has been employed previously in FTIR vibrational circular dichroism experiments (*17, 18*). The amplitude of the sinusoidal oscillations is increasing with energy; this deviation from the theoretically expected functional form can be attributed to a combination of slight errors in the phase correction and the variation with wavelength of the differential reflectivity of the Cr substrate. It is important to remember that the differential reflectance spectrum will have contributions from both the thin film and the substrate; in some instances, the wavelength dependence of the substrate differential reflectivity will be quite severe.

Figure 8B displays an expanded view of the differential reflectance spectrum from 1000 to 2000 cm^{-1}. The smooth sinusoidal background due to the wavelength dependence of the PEM can be fit by either eq 9 or a simple second-order polynomial expansion; normalization of the differential reflectivity spectrum to this background leads to the corrected spectrum in Figure 8C. The level base line in this spectrum demonstrates that a background normalization can be obtained in these PM-FTIR measurements without the need of a reference sample spectrum. Note also that the spectral region displayed in Figure 8C includes the region where bands due to the bending vibration of vapor-phase water occur; this spectrum was obtained without the assiduous purging of the FTIR spectrometer or sample compartment. For standard grazing incidence reflectance measurements, the elimination of atmospheric water bands due to variations between the sample and reference spectra can be a limitation to the spectral sensitivity in this wavelength region. Since the atmospheric water absorbs s-polarized and p-polarized infrared light equally, the PM-FTIR measurement is relatively insensitive to the presence of trace atmospheric water in the instrument.

To demonstrate the applicability of this method to the infrared spectra of adsorbed monolayers, the CH stretching region of the PM-FTIR differential reflectance spectra from two spontaneously organized monolayers is shown in Figures 9 and 10. For both of these spectra, the PEM was set to 3.15 μm and the sinusoidal background from the modulator was removed by normalization to the theoretical background. Figure 9 is the differential reflectance spectrum of an organized monolayer of octadecanethiol adsorbed onto a polycrystalline gold plug, and Figure 10 is the reflectance spectrum of an organized monolayer of arachidic acid adsorbed onto a 300-nm vapor-deposited silver film. In both cases, the sensitivity is sufficient to observe both the methylene and methyl CH stretching bands from the monolayer, and the band positions and relative intensities are in agreement with the p-polarized reflectance spectra of these compounds obtained previously by other groups (*2*).

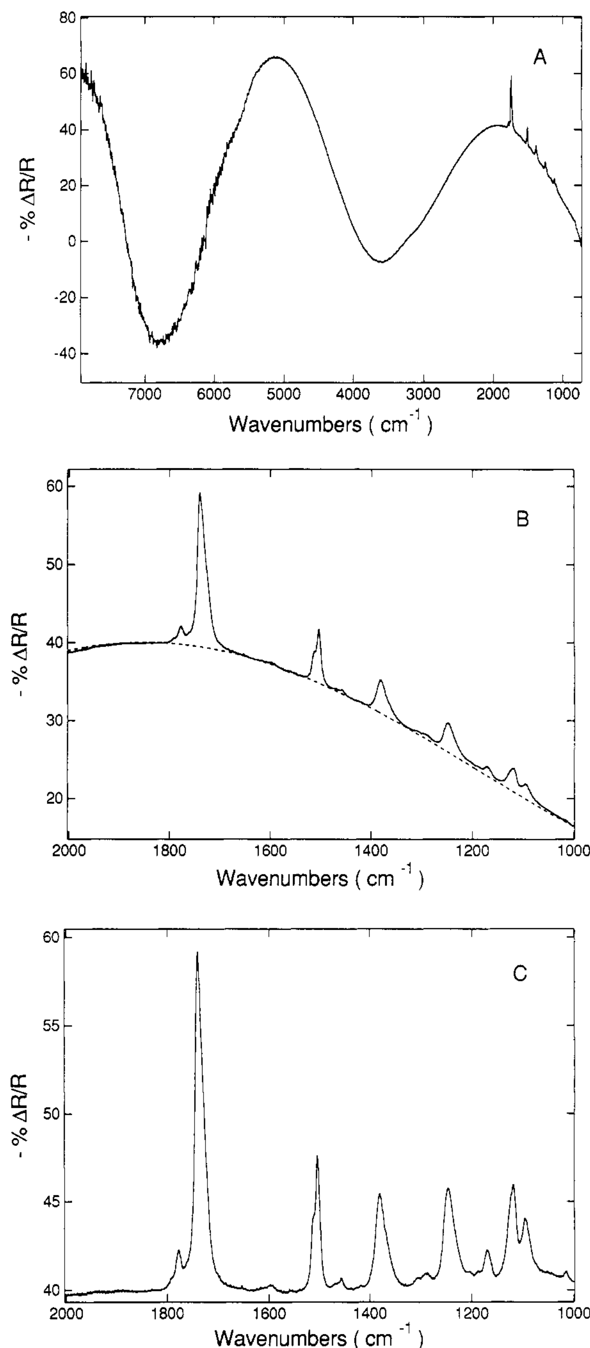

Figure 8. PM-FTIR differential reflectance spectrum from a 15-nm polyimide thin film adsorbed onto a vapor-deposited polycrystalline chromium substrate: (A) the complete spectrum from 750 to 7899 cm^{-1}; (B) an enlargement of the region 1000–2000 cm^{-1}; (C) the region 1000–2000 cm^{-1} after normalization to a theoretical background curve.

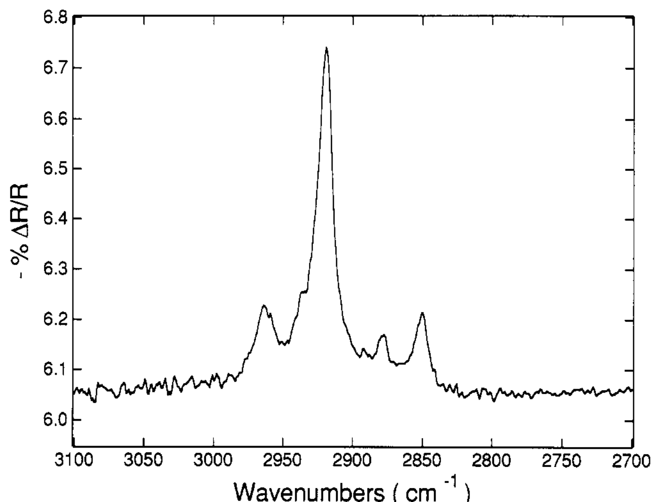

Figure 9. CH-streching region of the PM-FTIR differential reflectance spectrum from a spontaneously organized monolayer of octadecanethiol adsorbed onto a polycrystalline gold substrate.

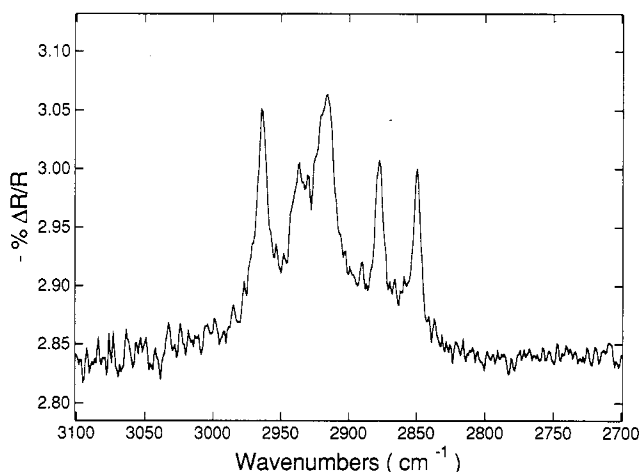

Figure 10. CH-streching region of the PM-FTIR differential reflectance spectrum from a spontaneously organized monolayer of arachidic acid adsorbed onto a vapor-deposited polycrystalline silver substrate.

The use of real-time sampling electronics in obtaining the PM-FTIR differential reflectance spectra has several advantages as compared to both p-polarized reflectance measurements and the conventional PM-FTIR lock-in amplifier methodology. The first is that with the optical geometry described in this paper the PM-FTIR measurements required no reference sample for a background. For monolayer samples, the reference sample employed in obtaining the p-polarized reflectance spectra must be scrupulously clean to avoid negative bands due to residual adsorption of impurities. In addition, the PM-FTIR experiments to date that have utilized a lock-in amplifier have required a background spectrum in order to remove any instrumental artifacts. Indeed, some of the original PM-FTIR measurements that employed reference samples displayed negative bands due to such impurities (*11*, *12*). The use of polarization-insensitive optics after the sample in the PM-FTIR experiments presented here along with the mathematical normalization procedure circumvents the need for a reference sample and thus avoids any impurity problems in the spectrum of the "bare" surface.

In addition to obviating the need for a background spectrum, the signal level and acquisition time for the PM-FTIR measurements are affected by the use of the real-time sampling electronics. Of course, with no background spectrum, the time required to obtain a reflectance spectrum is cut in half. An additional time effect is that the interferometer can be run at 2–3 times the mirror velocity employed in the lock-in amplifier measurements. The interferometer employed in our experiments was found to be significantly more stable at these higher velocities, presumably due to the removal of extraneous vibrational noise by shifting of the modulation frequencies out of the low-frequency (<1 kHz) acoustic range. The modulated signal obtained with real-time sampling is usually greater than that obtained with the lock-in amplifier experiment due to the shape of the modulation waveform. The lock-in amplifier only samples the modulation at 74 kHz, whereas measurement of the IR signal at 0° and 90° in each modulation cycle includes contributions from the higher harmonics (Figure 4). A final difference between the two PM-FTIR experiments is that the lock-in amplifier experiment is easily overloaded by the differential reflectivity of the metal substrate. To avoid this effect, previous groups have included a salt plate before the detector at nonnormal incidence to balance the metallic differential reflectivity (*12*). In the real-time measurement, this dc offset is subtracted electronically before amplification.

V. CONCLUSIONS

In summary, in this paper we have described a new implementation of the PM-FTIR method for obtaining the differential reflectance spectrum of thin films and monolayers adsorbed onto metal surfaces. Novel real-time electronics that sample the interferogram during each modulation cycle generate the average and difference FTIR reflectance spectra while the mirror is scanned at normal velocities. The theoretical wavelength dependence of the PM-FTIR spectra for the case of the real-time sampling measurement compares favorably to that obtained experimentally. Knowledge of this wavelength dependence and the use of polarization-independent optics after the metal surface lead to the acquisition of a differential reflectance spectrum over a wide bandwidth without the need for a reference sample. Spectra of a thin polyimide film and of spontaneously organized monolayers of octadecanethiol and arachidic acid demonstrate that the sensitivity of the method is sufficient for application of the technique to structures employed in chemical sensors, lithographic films, and thin film optical devices (*19*). Moreover, the surface sensitivity of this method makes it ideal for observation of real-time deposition processes and surface reactions, such as in electrochemical systems (*14*).

ACKNOWLEDGMENT

We thank Denise Denton and Milan Buncick for the polyimide sample.

LITERATURE CITED

(1) Swalen, J. D.; Rabolt, J. F. *Fourier Transform Infrared Spectrosc.* *1985*, *4*, 283.
(2) Porter, M. D. *Anal. Chem.* **1988**, *60*, 1143A.
(3) (a) Greenler, R. G. *J. Chem. Phys.* **1966**, *44*, 310. (b) Greenler, R. G. *J. Chem. Phys.* **1969**, *50*, 1963.
(4) Rabolt, J. F.; Burns, F. C.; Schlotter, N. E.; Swalen, J. D. *J. Chem. Phys.* **1983**, *78*, 946.
(5) (a) Allara, D. L.; Nuzzo, R. G. *Langmuir* **1985**, *1*, 52. (b) Schlotter, N. E.; Porter, M. D.; Bright, T. B.; Allara, D. L. *Chem. Phys. Lett.* **1986**, *132*, 93.
(6) (a) Gun, J.; Iscovici, R.; Sagiv, J. *J. Colloid Interfacial Sci.* **1984**, *101*, 201. (b) Gun, J.; Sagiv, J. *J. Colloid Interface Sci.* **1986**, *112*, 457.
(7) (a) Nuzzo, R. G.; Fusco, F. A.; Allara, D. L. *J. Am. Chem. Soc.* **1987**, *109*, 2358. (b) Porter, M. D.; Bright, T. B.; Allara, D. L.; Chidsey, C. E. D. *J. Am. Chem. Soc.* **1987**, *109*, 3559. (c) Troughton, E. B.; Bain, C. D.; Whitesides, G. M.; Nuzzo, R. G.; Allara, D. L.; Porter, M. D. *Langmuir* **1988**, *4*, 365.
(8) Golden, W. G. *Fourier Transform Infrared Spectrosc.* **1985**, *4*, 315.
(9) (a) Golden, W. G.; Dunn, D. S.; Overend, J. *J. Catal.* **1981**, *71*, 395. (b) Golden, W. G.; Saperstein, D. D.; Severson, M. W.; Overend, J. *J. Phys. Chem.* **1984**, *88*, 572.
(10) Pang, K. P.; Benziger, J. B.; Soriaga, M. P.; Hubbard, A. T. *J. Phys. Chem.* **1984**, *88*, 4583.
(11) Dowry, A. E.; Marcott, C. *Appl. Spectrosc.* **1982**, *36*, 414.
(12) Golden, W. G.; Saperstein, D. D. *J. Electron Spectrosc. Relat. Phenom.* **1983**, *30*, 43.
(13) Buffeteau, T.; Desbat, B.; Turlet, J. M. *Mikrochim. Acta* [*Wien*] **1988**, *2*, 23.

(14) (a) Golden, W. G.; Kunimatsu, K.; Seki, H. *J. Phys. Chem.* **1984**, *88*, 1275. (b) Kunimatsu, K.; Golden, W. G.; Seki, H.; Philpott, M. R. *Langmuir* **1985**, *1*, 245. (c) Kunimatsu, K.; Samant, M.; Seki, H.; Philpott, M. R. *J. Electroanal. Chem. Interfacial Electrochem.* **1988**, *243*, 203.
(15) Green, M. J.; Barner, B. J.; Corn, R. M. Unpublished results.
(16) Hipps, K. W.; Crosby, G. A. *J. Phys. Chem.* **1979**, *83*, 555.
(17) (a) Nafie, L. A.; Diem, M. *Appl. Spectrosc.* **1979**, *33*, 130. (b) Nafie, L. A.; Vidrine, D. W. *Fourier Transform Infrared Spectrosc.* **1982**, *3*, 83.
(18) McCoy, C. A.; de Haseth, J. A. *Appl. Spectrosc.* **1988**, *42*, 336.
(19) Swalen, J. D.; Allara, D. L.; Andrade, J. D.; Chandross, E. A.; Garoff, S.; Israelachvili, J.; McCarthy, T. J.; Murray, R.; Pease, R. F.; Rabolt, J. F.; Wynne, K. J.; Yu H. *Langmuir* **1987**, *3*, 932.

RECEIVED for review July 27, 1990. Accepted October 5, 1990. We gratefully acknowledge the support of the National Science Foundation in this study.

X-ray Photoelectron Spectroscopy Sputter Depth Profile Analysis of Spatially Controlled Microstructures in Conductive Polymer Films

Susan G. MacKay,[1] Mohammed Bakir, Inga H. Musselman,[2] Thomas J. Meyer, and Richard W. Linton*

Chemistry Department, University of North Carolina—Chapel Hill, Chapel Hill, North Carolina 27599-3290

X-ray photoelectron spectroscopy (XPS) sputter depth profiling of Ag-doped poly[Fe(4-vinyl-4′-methyl-2,2′-bipyridyl)$_2$(CN)$_2$]–poly(4-vinyl-4′-methyl-2,2′-bipyridyl) is described. These conductive polymer films are doped with Ag^I via soaking, and the distribution and oxidation state of the Ag dopants are modified by electrochemical reduction. XPS is evaluated for its ability to quantitatively profile the induced concentration gradients of Ag sites (<1 atomic %) in these thin (<1000 Å) films. XPS profiles of three different induced gradients correlate well with the predicted microstructures. Ion beam damage effects during depth profiling are evaluated in terms of preferential sputtering, sputter-induced chemical changes, and native versus sputter-induced roughness. Scanning tunneling microscopy (STM) is employed to correlate the achievable XPS depth resolution to the sputter-induced roughness. XPS provides both chemical speciation and atomic concentration information used to monitor the surface composition of these films during each step of the modification process.

INTRODUCTION

The ability to create spatially controlled microstructures in thin polymer films is critical for applications in electrocatalysis, chemical sensors, and chemically based microelectronics (*1–3*). Analytical characterization involves correlating film design and fabrication methods with spectroscopic techniques capable of yielding both spatial and lateral information. Problems in analyzing the polymeric films arise from the fact that these systems typically involve low concentrations (<1 atomic %) of metal dopants in thin (<1000 Å) films. Our previous work in profiling metal dopants in conductive films involved the use of sputter depth profiling by secondary ion mass spectrometry (SIMS) (*4, 5*). However, while SIMS has superior detection limits, it is often difficult to extract accurate and quantitative spatial information from a SIMS depth profile due to the presence of matrix effects including interfacial ion yield transients (*6*). Therefore, in cases where the dopant concentration is in the percent range, it is possible to use surface spectroscopic techniques which are less susceptible to matrix effects and thus more quantitative. One such technique is X-ray photoelectron spectroscopy (XPS). Recent advances in instrumentation have made XPS coupled with ion sputtering a practical technique for thin-film depth profiling (*7*).

In this study, poly[Fe(vbpy)$_2$(CN)$_2$]–poly(vpby) (vbpy = 4-vinyl-4′-methyl-2,2′-bipyridyl) films were doped with Ag^+ as $AgNO_2$, whose spatial location can be manipulated through the application of a negative potential to the electrode and reduction of Ag^+ to Ag^0. XPS was used to profile the distribution of metal sites in these thin (<1000 Å) conductive films. The XPS technique was evaluated for its ability to provide both chemical information and quantitative composition versus depth profiles for metallopolymeric films. While the experiments outlined in this study concentrate on a Ag-doped system, these films can be doped with a variety of metals including Pd, which is used in electrocatalytic applications.

EXPERIMENTAL SECTION

Apparatus. XPS spectra were acquired by using a Perkin-Elmer Physical Electronics Model 5400 XPS instrument equipped with a differentially pumped Ar^+ ion gun. The operating conditions of the XPS instrument were as follows: MgKα anode, 15 kV, 400 W; hemispherical analyzer pass energy, 35 eV; angle of collection, 45°; analysis area, 1 mm^2; sputter crater, 0.1 cm^2; ion beam energy, 4 keV Ar^+; ion dose rate, $\sim 1 \times 10^{14}$ ions cm^2/s. Profilometry was used to determine the sputter rate in a homogeneously doped film and was 180 ± 50 Å/min. The speciation studies were based on binding energy data acquired by measuring peak positions and charge referencing to C1s at 284.6 eV. The N1s windows were further reduced by using a Gaussian–Lorentzian curve fit routine with a Shirley background subtraction. Quantitative XPS information was obtained by using empirical relative sensitivity factors (*8*).

Scanning tunneling microscopy (STM) measurements were performed on the surface of the Ag^+-doped poly[Fe(vbpy)$_2$(CN)$_2$]–poly(vbpy) films by using a Nanoscope I (Digital Instruments, Inc.) STM instrument with a long-range piezoelectric tube scanner that was calibrated by the manufacturer. This system was modified to include digital scanning and data acquisition using an 80386-based PC/AT computer. A Pt/Ir tip

[1] Present address: Perkin-Elmer Corp., Physical Electronics Division, Eden Prairie, MN 55344.
[2] Department of Materials Science and Engineering and Precision Engineering Center, North Carolina State University, Raleigh, NC 27695.

0003-2700/91/0363-0060$02.50/0 © 1990 American Chemical Society